Multidiscipline Modeling in Mat. and Str., Vol. XX, No. XX, pp. 1-30(XXXX)

Also available online-www.vsppub.com

A COMPUTATIONAL INVESTIGATION OF VARIOUS WATER-INDUCED EXPLOSION MITIGATION MECHANISMS

M. Grujicic[1*], B. Pandurangan[1], C. L. Zhao[1] and Bryan Cheeseman[2]
[1] *Department of Mechanical EngineeringClemson University, Clemson SC 29634-0921*
[2] *Army Research Laboratory – Survivability Materials Branch Aberdeen, Proving Ground, MD 21005-5069*

Received 2 March 2006; accepted 3 May 2006

Abstract—Interactions of the detonation-product gas, shell-casing fragments, soil ejecta and various other debris with bulk water barriers surrounding the explosive have been demonstrated to have a potentially major beneficial effect in mitigation of the effects of an explosion. In the present work, various computational methods ranging from those based on thermo-chemistry of the detonation/combustion chemical reactions to those involving transient, nonlinear-dynamics based mechanical interactions between detonation products, air and water are used to better understand and quantify the beneficial effects of various potential explosion-mitigation mechanisms. In particular, the absorption of the detonation energy by water, water-aerosolization induced reduction in the shock speed, transfer of momentum from the explosion products to water and deceleration/suppression of the combustion reactions are examined computationally. The results obtained show that water evaporation which consumes a substantial portion of the detonation energy plays a dominant role in the overall water-induced explosion-mitigation process. The detonation-product-to-water momentum transfer which causes water aerosolization, on the other hand, is found to be a key prerequisite for efficient explosion mitigation.

Keywords: High-Energy Explosives, Detonation, Mitigation, Water Barriers, AUTODYN

NOMENCLATURE

a	-	Radius of the droplet
a_1	-	Constant in Polynomial Equation of State
A	-	Liquid/gas surface area
A_1	-	Constant in JWL Equation of State
A_2	-	Pre-exponential term in Arrhenius reaction rate equation
a	-	Mass Fraction
b	-	Constant in Polynomial Equation of State
B	-	Bulk modulus

* E-mail: mica.grujicic@ces.clemson.edu
Tel: (864) 656-5639, Fax: (864) 656-4435

Report Documentation Page

Form Approved
OMB No. 0704-0188

1. REPORT DATE	2. REPORT TYPE	3. DATES COVERED
2007		**00-00-2007 to 00-00-2007**

4. TITLE AND SUBTITLE	5a. CONTRACT NUMBER
A Computational Investigation of Various Water-Induced Explosion Mitigation Mechanisms	5b. GRANT NUMBER
	5c. PROGRAM ELEMENT NUMBER
6. AUTHOR(S)	5d. PROJECT NUMBER
	5e. TASK NUMBER
	5f. WORK UNIT NUMBER
7. PERFORMING ORGANIZATION NAME(S) AND ADDRESS(ES) **Celmson University,Department of Mechanical Engineering,Clemson,SC,29634**	8. PERFORMING ORGANIZATION REPORT NUMBER
9. SPONSORING/MONITORING AGENCY NAME(S) AND ADDRESS(ES)	10. SPONSOR/MONITOR'S ACRONYM(S)
	11. SPONSOR/MONITOR'S REPORT NUMBER(S)

12. DISTRIBUTION/AVAILABILITY STATEMENT
Approved for public release; distribution unlimited

13. SUPPLEMENTARY NOTES
Multidiscipline Modeling in Materials and Structures, 3, pp. 185-212, 2007

14. ABSTRACT
Interactions of the detonation-product gas, shell-casing fragments, soil ejecta and various other debris with bulk water barriers surrounding the explosive have been demonstrated to have a potentially major beneficial effect in mitigation of the effects of an explosion. In the present work various computational methods ranging from those based on thermo-chemistry of the detonation/combustion chemical reactions to those involving transient, nonlinear-dynamics based mechanical interactions between detonation products, air and water are used to better understand and quantify the beneficial effects of various potential explosion-mitigation mechanisms. In particular, the absorption of the detonation energy by water, water-aerosolization induced reduction in the shock speed, transfer of momentum from the explosion products to water and deceleration/suppression of the combustion reactions are examined computationally. The results obtained show that water evaporation which consumes a substantial portion of the detonation energy plays a dominant role in the overall water-induced explosion-mitigation process. The detonation-product-to-water momentum transfer which causes water aerosolization, on the other hand, is found to be a key prerequisite for efficient explosion mitigation.

15. SUBJECT TERMS

16. SECURITY CLASSIFICATION OF:			17. LIMITATION OF ABSTRACT	18. NUMBER OF PAGES	19a. NAME OF RESPONSIBLE PERSON
a. REPORT **unclassified**	b. ABSTRACT **unclassified**	c. THIS PAGE **unclassified**	**Same as Report (SAR)**	**30**	

B_1 - Constant in JWL Equation of State
b - Temperature exponent in Arrhenius reaction rate equation
C - Speed of sound
d - Diameter of water droplets
D - Diffusion Coefficient
E - Internal energy
e - True Strain
f - Volume fraction
G - Gruneisen Parameter
$?$ - Constant-pressure to constant-volume specific heats ratio
K_m - Liquid-to-vapor mass transfer coefficient
M_s - Mach number
m - Thermal Softening Exponent
M - Molecular mass
$\dot{m}$ - Mass evaporation rate
m - Compression Ratio
n - Strain Hardening Exponent
N - Number of Spherical Droplets
n - Specific Volume
P - Pressure
Q - Latent Heat of Vaporization for water
r_{H_2O} - Radius of Water droplets
R_1 - Constant in JWL Equation of State
R_2 - Constant in JWL Equation of State
$?$ - Density
s - Surface Energy
T - Temperature
V - Total volume
u - Velocity
w - Constant in JWL Equation of State
We - Weber Number
X - Molar fraction

Subscripts

air - Air related quantity
$C(s)$ - Carbon (solid) related quantity
CO - Carbon-monoxide related quantity
g - Gas related quantity
H_2O - Water quantity
l - Liquid related quantity
mix - Mixture quantity
N_2 - Nitrogen related quantity
p - Plastic state related quantity
st - Steel related quantity
o - Initial condition
$room$ - Property at room temperature
$melt$ - Property at melting point

b - Break-up event
d - Droplet related quantity

1. INTRODUCTION

It is well established that bulk water barriers placed in the vicinity of high-energy explosives in either a confined environment or an unconfined environment can significantly mitigate the effects of explosions by reducing the quasi-static gas pressure and impulse (in some cases up to 90%) [e.g.1-10]. This explosion mitigation effect of water is of major importance for the safety of explosive production and storage facilities, protection of military structures, vehicles, personnel and safe demolition of employed unexploded ordnance. While the explosion mitigation effect of water is clearly demonstrated, the underlying physical mechanism or mechanisms are not that well understood. For example, Keenan and Wager [11] suggest that blast waves from the explosion cause the water to aerosolize and upon mixing with the hot detonation gases to evaporate. This causes the detonation gases to cool down and the gas pressure to decrease. In addition, the resulting lower temperatures of the gases hamper the progress of the secondary oxidation reaction of the detonation products in oxygen-deficient explosives further reducing the gas pressure. Ericksson and Vretblad [12], on the other hand, observed that the latter effect may not be significant since no major differences in the explosion mitigation effect by bulk water was observed in highly oxygen-deficient explosives such as TNT and oxygen non-deficient explosives. Also a frequently cited mechanism for water-induced explosion mitigation which considers bulk water as a passive barrier that can absorb some of the energy and momentum of the explosion products is not well understood [13].

The objective of the present work is to carry out various computational analyses in order to help better understand and quantify the contributions of various mechanisms to the explosion mitigation effect of bulk water. It should be noted that the term "*bulk water*" is used throughout the paper to indicate that initially water is present in a bulk form, however, as will be discussed later, the interaction of the explosion products with bulk water can cause the water to aerosolize, i.e. break up into micron-size droplets. Also the term "*bulk water*" is used to make a distinction relative to the direct use of water mist.

The organization of the paper is as follows. A brief description of various mathematical models used to analyze the different mechanical/thermal and chemical aspects of a detonation process in the presence of bulk water and an overview of the constitutive laws governing the response of various materials when subjected to blast loading are discussed in Sections 2.1-2.3. The results obtained in the present work are presented and discussed in Section 3. The main conclusions resulting from the present work are summarized in Section 4.

2. COMPUTATIONAL ANALYSES

2.1. General Consideration

As mentioned earlier, various water-induced explosion-mitigation effects are analyzed computationally in the present work using several analytical and numerical techniques

ranging from those emphasizing thermo-chemical aspects of the detonation process to those dealing with transient; nonlinear-dynamics based mechanical interactions between detonation products, air and water. In general, thermo-chemical analyses are carried out using MATLAB, a general purpose mathematical, computational and visualization package [14]. Since this computer package is widely used and well-known, it is not discussed any further in the present paper. The transient nonlinear-dynamics based mechanical interactions between various materials participating in a detonation process are analyzed using AUTODYN, a state-of-the-art non-linear dynamics computational code [15]. A brief overview of this code is given in next section.

2.2. Transient Nonlinear-Dynamics Calculations

All the transient nonlinear-dynamics mechanical interactions between various materials attending a detonation process are analyzed computationally using AUTODYN, a state-of-the-art nonlinear dynamics modeling and simulation software [15]. In this section, a brief overview is given of the basic features of AUTODYN, emphasizing the aspects of this computer program which pertain to the problem at hand.

AUTODYN is a fully integrated engineering analysis computer code which is particularly suited for modeling the explosion, blast, impact and penetration events. Codes such as AUTODYN are commonly referred to as "*hydrocodes*". Within the code, the appropriate mass, momentum and energy conservation equations coupled with the materials modeling equations and subjected to the appropriate initial and boundary conditions are solved. The numerical methods used for the solution of these equations involve finite difference, finite volume and finite element methods and the choice of the method used (i.e. "*processor*" as referred to in AUTODYN) depends on the physical nature of the problem being studied. The power of AUTODYN is derived mainly from its ability to handle complex problems in which different regions can be analyzed using different methods such as the Lagrange processor (typically used for solid continuum and structures) and the Euler processor (commonly used for modeling gases, liquids or solids subject to large deformations). While the available Euler processor provides multi-material capabilities, an additional Euler-FCT single material processor in which materials are combined to a single material using a Flux Corrected Transport (FCT) approach is available to help handle computationally intensive multi-material blast phenomena.

Additional methods available in AUTODYN include: an ALE (Arbitrary Lagrange Euler) processor capable of carrying out an automatic rezoning (remeshing) of distorted grids; a Shell processor designated for modeling thin structures and a gridless SPH (Smooth Particle Hydrodynamics) processor which does not suffer from a grid tangling problem (typically encountered in Lagrangian processor) and does not entail the use of an unphysical erosion algorithm (removal of highly distorted grids to help the numerical procedure).

2.3. Materials Constitutive Models

Hydrodynamic computer programs such as AUTODYN [15] are capable of predicting an unsteady, dynamic motion of a material system by solving the appropriate mass, momentum and energy conservation equations, subjected to the associated initial and boundary conditions. However, for the aforementioned boundary value problem to be

fully defined, additional relations between the flow variables (pressure, density, energy, temperature, etc.) have to be defined. These additional relations typically involve an equation of state, a strength equation and a failure equation for each constituent material. These equations arise from the fact that, in general, the total stress tensor can be decomposed into a sum of a hydrostatic stress (pressure) tensor (which causes a change in the volume/density of the material) and a deviatoric stress tensor (which is responsible for the shape change of the material). An equation of state then is used to define the corresponding functional relationship between pressure, density and internal energy (temperature), while a strength relation is used to define the appropriate equivalent plastic-strain, equivalent plastic-strain rate, and temperature dependences of the equivalent deviatoric stress (or some function of it). In addition, a material model generally includes a failure criterion, i.e. an equation describing the (hydrostatic or deviatoric) stress and/or strain condition which, when attained, causes the material to fracture and loose its ability to support normal and shear stresses.

In the present work the following materials are utilized within the computational domain: air, a high-energy explosive (e.g., TNT), water and 4340 steel. In the following sections, a brief description is given of the models used for each of the four constituent materials.

2.3.1 Air

Air is modeled as an ideal gas and, consequently, its equation of state is defined by the ideal-gas gamma-law relation as [15]:

$$P = (\gamma - 1)\frac{\rho}{\rho_0} E \tag{1}$$

where P is the pressure, γ the constant-pressure to constant-volume specific heats ratio (=1.4 for a diatomic gas like air), ρ_0 (=1.225kg/m^3) is the initial air density, and ρ is the current density. For Eq.(1) to yield the standard atmosphere pressure of 101.3kPa, the initial specific internal energy E is set to 253.4kJ/m^3 which corresponds to the air mass specific heat of 717.6J/kg·K and a reference temperature of 288.2K.

Since air is a gaseous material and has no ability to support either shear stresses or negative pressures, no strength or failure relations are required for this material.

2.3.2 High-Energy Explosives

High-energy explosives like TNT are chemical substances which when subjected to a particular mechanical or thermal stimulus, can undergo a chemical reaction (or a series of chemical reactions) releasing, very rapidly (at a time scale of microseconds), a large amount of energy. The whole process comprised of chemical reactions taking place within the high-energy explosive and the associated release of energy is generally referred to as detonation. Within a hydrodynamic code, detonation is typically assumed to take place instantaneously at each material point within the high-energy explosive when such points are properly stimulated. In other words, as a result of initial detonation at predefined detonation locations (points, lines or planes), detonation waves are generated which extend into the unreacted explosive material instantaneously liberating the energy of chemical reactions and transforming the explosive material into gaseous

detonation products at each point swept by the detonation wave.

Mathematical description of a detonation-induced shock wave is based on the normal Rankine-Hugoniot mass, momentum and energy conservation equations which relate the hydrodynamic quantities (density, pressure, energy) across the discontinuity (a shock wave) [16]. The only difference between the Rankine-Hugoniot equations for a shock wave in a non-explosive material and their counterparts for a detonation wave is the inclusion of a chemical energy term (initially residing as a chemical energy term in the explosive) in the energy equation.

For a high-energy explosive material in an initial condition defined by pressure P_0, density r_0 and specific volume $v_0 = 1/r_0$, the line denoted as "*Hugoniot Curve*" in Fig.1 represents the locus of all (*P*, *v*) states attainable from the initial (P_0, v_0) state during detonation. It should be noted that, in contrast to the case of a non-explosive material, the Hugoniot curve does not pass through the initial explosive state (P_0, v_0) but it is rather shifted toward higher pressures due to the chemical energy release accompanying detonation of the explosive material. In addition to the Hugoniot curve, an additional line denoted as the "*Rayleigh Line*" is depicted in Fig.1. This line corresponds to the all (*P*, *v*) states of the detonation products consistent with a given detonation-wave speed and the Rankine-Hugoniot mass and momentum conservation equations. It should be noted that there is a separate Rayleigh line for each value of the detonation-wave speed. The Rayleigh line depicted in Fig.1 is the line associated with the minimum detonation speed which, at the same time, yields the (*P*, *v*) states of the detonation-product which are consistent with the Hugoniot curve. The point of tangency of the Rayleigh line and the Hugoniot curve is generally referred to as the Chapman-Jouget point and defines both the value of the detonation speed and the corresponding (*P*, *v*) state of the detonation products.

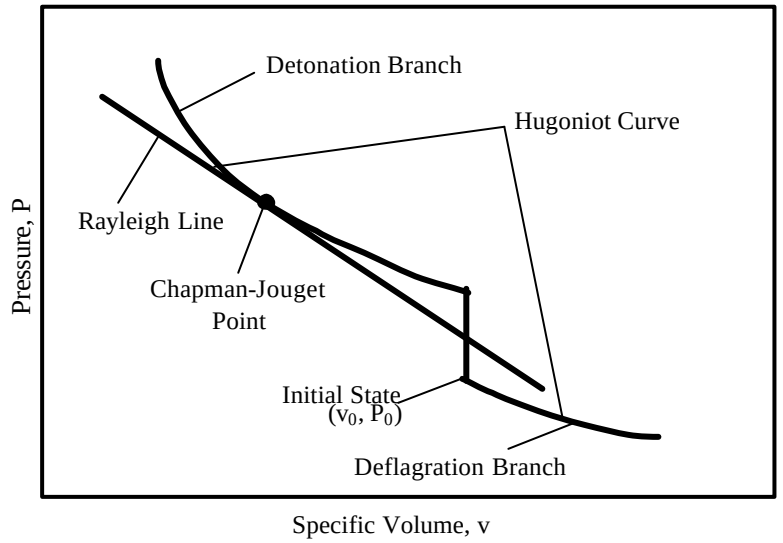

Fig.1. Pressure vs. specific volume relations in a high-energy explosive material. Please see the text for details.

The equation of state for an explosive then defines a locus of (P, v) states associated with expansion (or compression) of the detonation products. One of these states is clearly the initial state of the detonation products corresponding to the Chapman-Jouget point. Since the detonation products are generally associated with very high temperatures, their expansion/compression does not give rise to a significant change in entropy. Hence, it is generally accepted that, at least in the vicinity of the Chapman-Jouget point, the equation of state prescribes the states which are consistent with the P-v adiabat passing through the Chapman-Jouget point. The remainder of the P-v curve corresponding to the expansion of the detonation products is generally obtained by matching the area under the P-v curve up to large expansions and down to atmospheric pressure with the experimentally measured work of detonation.

The Jones-Wilkins-Lee (JWL) equation of state is used for a high-energy explosive in the present work since that is the preferred choice for the equation of state for high-energy explosives in most hydrodynamic calculations involving detonation. The JWL equation of state is defined as [17, 18]:

$$P = A_1\left(1-\frac{w}{R_1 v}\right)e^{-R_1 v} + B_1\left(1-\frac{w}{R_2 v}\right)e^{-R_2 v} + \frac{wE}{v} \tag{2}$$

where the constants A_1, R_1, B_1, R_2 and w for a given high-energy explosive like TNT are defined in the AUTODYN materials library and v is the specific volume of the material. As explained earlier, within a typical hydrodynamic analysis, detonation is modeled as an instantaneous process which converts unreacted explosive into gaseous detonation products and detonation of the entire high-energy explosive material is typically completed at the very beginning of a given simulation. Consequently, no strength and failure models are typically used for the high-energy explosives.

2.3.3 Water

Separate equations of state are used for water depending on whether water is subjected to expansion or compression. When water is subjected to expansion, a two-phase equation of state proposed by Morgan [19] is used while in compression a polynominal type of equation of state [15] is used.

The two-phase equation of state for water is applicable when water is expanded from its initial state or in a single-phase (liquid or vapor) region or in the two-phase (water+vapor) region. As shown in Fig.2, the pressure/specific-volume plane at the expansion side ($v > v_0$, v_0 the initial specific volume) is divided into two regions by the saturation curve. Above this curve water exists in a single-phase (liquid or vapor) state, while below the saturation curve the two phases coexist. Values for P, v, r, e and T along the saturation curve are known and are tabulated with the AUTODYN material database.

When the values of v and E place water in a single-phase region, pressure is defined by the Mie-Gruneisen equation of state in the form [15]:

$$P = P_r(v) + \frac{\Gamma_r(v)}{v}[E - E_r(v)] \tag{3}$$

where the reference quantities denoted with a subscript *r* are known and are associated with the saturation curve, while $\Gamma \equiv v(\partial P / \partial E)_v$ is the so-called Gruneisen gamma, whose values are also known along the saturation line.

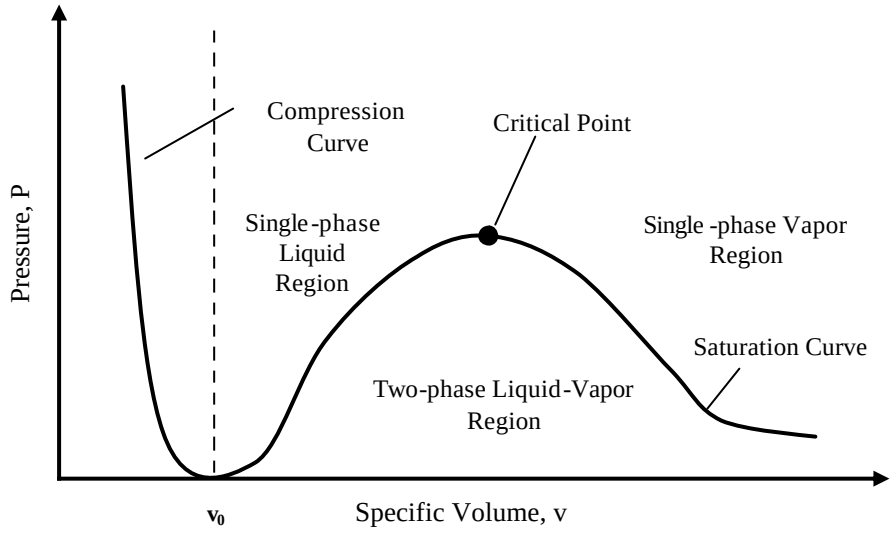

Fig.2. Pressure vs. specific volume relations for water used in the derivation of the two-phase equation of state. Please see the text for details.

When the values of *v* and *E* place water within a two-phase region, the volume and energy weighted average equations:

$$v = \alpha v_g + (1-\alpha)v_l \text{, and} \tag{4}$$

$$E = \alpha E_g + (1-\alpha)E_l \tag{5}$$

where α is the mass fraction of vapor and subscript *g* and *l* denote the gas phase and the liquid phase, respectively, are combined to yield:

$$\frac{v - v_g}{v_g - v_l} = \frac{E - E_g}{E_g - E_l} \tag{6}$$

Since the specific volumes and energies of the saturated liquid and vapor (v_l, E_l, v_g, E_g) are mutually constrained by the saturation curve, Eq. (6), defines the pressure (or temperature) for the given values of *v* and *E*.

When water is subjected to compression, the following polynomial equation of state is used:

$$P = a_1 m + a_2 m^2 + a_3 m^3 + (b_0 + b_1 m)\rho_o E \tag{7}$$

where $m = r / r_0 - 1$ is the compression, r_0 the initial density and the coefficients a_1, a_2, a_3, b_0 and b_1 are defined in the AUTODYN material library.

No strength model is used for water because water has very little ability to support a shear stress. However, in order to examine the possibility for water break-up into small droplets as a result of its interaction with the detonation gases, a minimum negative-pressure failure criterion is used. The magnitude of the critical minimum failure-pressure is varied in order to examine its effect on the results of the computational analyses.

2.3.4 4340 Steel

For inert solid materials like 4340 steel, a linear type of equation of state is typically used which assumed a Hooke's law type relationship between the pressure, *P*, and the volume change $m = \left(\frac{r}{r_0} - 1 \right)$ as:

$$P = Bm \tag{8}$$

where *K* is the bulk modulus of the material. Within the AUTODYN material database, the initial material density r_0, the bulk modulus *B*, the specific heat, C_p and the reference temperature (T_{ref}) are defined for 4340 steel.

To represent the constitutive response of 4340 steel under deviatoric stress, the Johnson-Cook model is used. This model is capable of representing the material behavior displayed under large-strain, high deformation rate, high-temperature conditions, of the type encountered in problems dealing with the interactions of detonation products and solid structures. Within the Johnson-Cook model, the yield stress is defined as:

$$Y = \left[A_{st} + B_{st} e_{p\,st}^{\,n} \right] \left[1 + C_{st} \log \dot{e}_{p\,st} \right] \left[1 - T_{H\,st}^{\,m} \right] \tag{9}$$

where $e_{p\,st}$ is the equivalent plastic strain, $\dot{e}_{p\,st}$ the equivalent plastic strain rate, A_{st} the zero plastic-strain, unit plastic-strain rate, room-temperature yield stress, B_{st} the strain hardening constant, n_{st} the strain hardening exponent, C_{st} the strain rate constant, m_{st} the thermal softening exponent and $T_H = (T - T_{room})/(T_{melt} - T_{room})$ a room temperature (T_{room}) based homologous temperature while T_{melt} is the melting temperature. All temperatures are given in degrees of Kelvin.

Since 4340 steel structures are generally subjected to compressive type of stresses, no failure model was used for the 4340 steel in the present work.

3. RESULTS AND DISCUSSION

In this section, the four most frequently cited water-induced explosion-mitigation mechanisms: (a) absorption of the detonation energy; (b) reduction of the shock speed; (c) detonation-product-to-water momentum transfer and (d) deceleration/suppression of combustion of the detonation products are analyzed using the underlying physical

principles. In addition, the results of numerical analyses of the four mechanisms are presented and discussed. In each case, an effort was made to quantify the effectiveness of the specific water-mitigation mechanism in reducing the pressure (and temperature) of the detonation-product gas-mixture. Such effectiveness is judged by both the magnitude of the effect and by the rate at which such effect takes place.

3.1 Absorption of the Detonation Energy

3.1.1 General Consideration

Due to its relatively large specific heat (~4.187kJ/kg·K) and a relatively large latent heat of evaporation (~2.25MJ/kg), water has an excellent ability to absorb energy of detonation (and combustion) of high-energy explosives. For comparison, the detonation energy of TNT is about 4.45MJ/kg while the combined energies of detonation and subsequent combustion of this oxygen-deficient explosive is about 4.45+10.22=14.67 MJ/kg. However, for the water to be able to absorb the detonation/combustion energy of a high-energy explosive at the explosion time scale of tens of microseconds to tens of milliseconds, the water must be present in the form of a mist (micron-size droplets) to ensure a fast explosion-products-to-water thermal energy transfer. In general, the mass evaporation rate of water, $\dot{m}_{H_2O}$, can be defined as:

$$\dot{m}_{H_2O} = K_m A_{H_2O} (P^{sat}_{H_2O} - X_{H_2O} P) \tag{10}$$

where K_m is the liquid-to-vapor mass transfer coefficient, A_{H_2O} the liquid/gas surface area, $P^{sat}_{H_2O}$ the water vapor saturation pressure, X_{H_2O} the molar fraction of water-vapor in the gas phase and P the pressure of the gas phase.

According to Eq. (10), the rate of evaporation scales linearly with the surface area of water being evaporated. The surface area of water dispersed into N spherical droplets of radius, r_{H_2O}, is related to the total water volume, V_{H_2O}, and to the droplet radius as:

$$A_{H_2O} = \frac{3V_{H_2O}}{r_{H_2O}} = \frac{3N\frac{4}{3}\pi r^3_{H_2O}}{r_{H_2O}} = N4\pi r^2_{H_2O} \tag{11}$$

The application of Eq. (11) shows that a single water sphere which has a volume of $1m^3$ and a surface area of $4.836m^2$ gives rise to a surface area of ~$200{,}000m^2$, if it is dispersed into spherical droplets with a radius r_{H_2O}=15μm. In accordance with Eq. (10), this would increase the evaporation rate by a factor of over 41,000.

3.1.2 A Thermo-chemical Analysis

Evaporation of the water droplets gives rise to a reduction in the temperature, and hence, the pressure of the hot detonation products and, as will be discussed later, can slow down or even prevent the subsequent combustion chemical reaction of the detonation products. To quantify the effect of water evaporation on temperature reduction of the

detonation products, a simple quantitative thermal energy balance analysis for the case of TNT, a high-energy explosive is carried out in this section.

TNT is a solid high-energy explosive with a chemical formula $C_7H_5N_3O_6$ which produces during detonation a gas mixture which is laden with solid-carbon soot and which has the following chemical composition in mole fractions: $X_{H_2O} = 0.227$, $X_{CO} = 0.318$, $X_{C(s)} = 0.318$ and $X_{N_2} = 0.136$. The initial temperature of the mixture is about 3500K. Temperature variation of the molar specific heats for the gas mixture constituents (as well as for molecular oxygen and carbon dioxide) are displayed in Fig.3. From the molecular weights of the mixture constituents, $M_{H_2O} = 18$, $M_{CO} = 28$, $M_{C(s)} = 12$ and $M_{N_2} = 28$, all in g/mol, the average molar specific heat, $C_{P,\,M,\,mix}$, and the average molecular weight, M_{mix}, of the mixture are computed as a mole-fraction weighted averages of the respective constituent quantities as:

$$C_{P,M,mix} = \sum_i X_i C_{P,M,i} \quad (i = H_2O, CO, C(s), N_2) \tag{12}$$

and

$$M_{mix} = \sum_i X_i M_i \quad (i = H_2O, CO, C(s), N_2) \tag{13}$$

The corresponding mass-based specific heat of the mixture is then obtained as:

$$C_{P,m,mix} = \frac{C_{P,M,mix}}{M_{mix}} \tag{14}$$

To quantify the effect of water evaporation on temperature reduction of the detonation-product gas mixture, the following energy balance equation is used:

$$m_{H_2O} \cdot C_{P,m,H_2O}(373 - 298) + m_{H_2O} \cdot Q_{evap,H_2O} = \int_{3500}^{T_{final}} m_{mix} \cdot C_{P,m,mix} dT \tag{15}$$

The left-hand side in Eq. (15) corresponds to the energy absorbed by a m_{H_2O} mass of water from its initial temperature (298K) till the point of boiling (T=373K) and during subsequent evaporation. The right-hand side of Eq. (15), on the other hand, corresponds to the energy given off by a M_{mix} mass of the hot detonation-product gas-mixture and is defined to take into account temperature dependence of the mixture specific heat, $C_{P\_m\_mix}$, in accordance with Fig.3.

When Eqs. (12) - (15) are applied to one kilogram of TNT and one kilogram of water and the following data are used for the mass specific heat and the mass evaporation energy of water: $C_{P,m,H_2O} = 4.187 kJ/kg \cdot K$ and $Q_{evap,H_2O} = 2.25 MJ/kg$, the final temperature of the mixture is obtained as $T_{final} = 2298K$. This finding shows that, if one kilogram of water can be evaporated for each kilogram of TNT detonated, the

temperature of the resulting detonation gas mixture would be reduced by $?T$=3500 - 2298 =1202K.

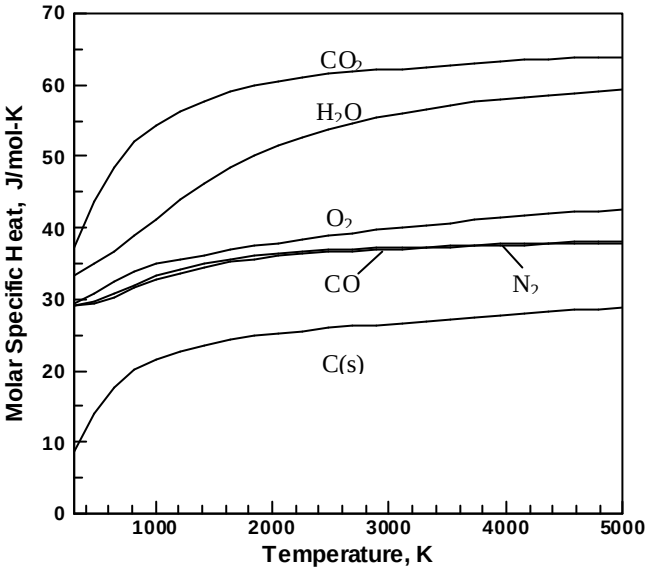

Fig.3. Temperature variation of the molar specific heat for a number of species attending detonation/combustion of TNT.

Clearly, water can be very efficient in reducing the temperature of the detonation-product gas-mixture. In fact, since the specific heat of the gas-mixture constituents decreases as their temperature is reduced in Fig.3, further increase in the relative amount of water would be even more effective in reducing the temperature of the detonation-product gas-mixture. As will be discussed later, a reduction in the temperature of the detonation-product gas-mixture can substantially reduce the rate of subsequent oxidation (combustion) of CO(g) and C(s) in the mixture or even prevent this reaction from taking place. Since, this reaction is associated with the formation of a fire-ball which advances with the detonation front and releases a substantial amount of thermal energy, its suppression is highly desirable from the explosion-mitigation stand point.

Previous experimental investigations [e.g. 1-10] have shown that the use of water barriers can reduce the peak hydrostatic pressure by as much as 90%. The computed water-induced reduction in the temperature of the detonation-product gas-mixture from ~3500K by ~1200K, would certainly give rise to a reduction in the pressure of the mixture. However, it is not clear that the reduction in the mixture temperature could solely account for the observed reduction of the peak hydrostatic pressure. If one assumes that the hydrostatic pressure of a gas mixture scales linearly with its temperature, as is the case for the ideal gas law (the use of ideal gas law might not be fully appropriate considering high pressure levels in the detonation-product gas-mixture), the observed temperature reduction would give rise to a pressure reduction in a range between 30-35%. While increasing the relative amount of water is expected to give rise to a further reduction in the gas-mixture temperature and pressure, the extent of this reduction may not be proportional to the amount of water since it depends on the ability

of the detonation-product gas-mixture to aerosolize the additional water.

As stated above, the use of the ideal gas law to predict the potential water-evaporation induced reduction in the gas-phase pressure may not be very reliable due to the attendent high pressure levels. Here we provide yet another estimate of this pressure reduction. In several experimental investigations [e.g. 10], it was established that the peak side-on (hydrostatic) pressure at a given point scales with the explosive total energy raised to a power of 1/3. If one treats the energy absorbed by water during evaporation as a means of reducing the total energy of the explosive, one can obtain another estimate for the water-induced pressure reduction.

As stated earlier the total energy of explosion for TNT which includes the heat of detonation and the heat of subsequent combustion is ~ 14.67MJ/kg TNT. Evaporation of 1kg of water consumes about 2.25MJ of energy, so that the effective total energy of TNT can be considered as 14.67-2.25=12.42MJ/kg TNT, a reduction of ~15% which would yield, according to the aforementioned correlation, a decrease in pressure of only ~ 5% per kg of water. If water completely suppresses the combustion reaction, on the other hand, the effective specific energy of TNT is reduced to 14.67-10.22-2.25=2.2MJ/kg TNT, a reduction of ~ 85%. The resulting pressure reduction is about 53%. It appears, hence, that for the water evaporation process to have a significant effect on gas-phase pressure reduction, it must cause cessation of the combustion reaction in oxygen-deficient explosives.

It should be noted that aerosolization of water also consumes some energy initially residing in the detonation-product gas-mixture. Namely, the formation of small water droplets is accompanied by a substantial increase in the energy stored at the surface of water. The surface energy of water is $0.072 J/m^2$ at room temperature and decreases to $\sim 0.060 J/m^2$ near the boiling point. As shown in the previous section, $1 m^3$ of water dispersed into 15μm-radius droplets have a total surface area of ~ $200{,}000 m^2$. Thus the energy absorbed by water in the aerosolization process is at most 0.072x 200,000 =14,400J/kg H_2O = 14.4 kJ/kg H_2O. This value is only a tiny fraction of the water evaporation energy (~2.25MJ/kg H2O) and, hence, can be neglected.

3.1.3 A Fluid-dynamic Analysis

According to Eq. (10), the evaporation rate of water is proportional to a temperature-dependent liquid-to-vapor mass transfer coefficient, K_m. To a great extent, the magnitude of K_m is controlled by the rate at which the heat is transferred from the detonation-product gas-mixture to the water droplets. The gas-mixture-to-water droplets heat transfer rate is, on the other hand, greatly affected by the extent of turbulence in the gas-phase stream. Furthermore, the presence of water droplets in the gas-phase stream is expected to have some effect on the extent of turbulence. In the early stages of the water break-up process, when large water droplets (fragments) are present, a general increase in the extent of turbulence is expected since water droplets can create turbulent regions in their wake. Conversely, in the later stages of the water break-up process, when micron-size water droplets are present, such droplets, due to their large density, would reduce flow fluctuations and, hence, lower the extent of turbulence. However, one must take into account the fact that due to high values of the evaporation rates, the life span of micron-size droplets is very short. While no quantitative analysis is carried out in the present work pertaining to the effects of water-droplets number density and size on the gas-to-water heat transfer coefficient, the discussion given earlier in this section

(specifically the presence of counter balancing phenomena) suggests that their effects are, perhaps, of a second order relative to the effect of enhanced surface area on the rate of evaporation of the water.

3.1.4 A Kinetic Analysis of Water Evaporation

The analyses presented above demonstrate that water evaporation has the potential for absorbing the substantial portions of the thermal energy carried by the detonation-product gases. However, for this potential to be fully utilized, water must be dispersed in the form of small-size droplets which can evaporate over a time-period of up to few tens of microseconds. In this section, we utilized several existing droplet evaporation models to assess the time for evaporation of the water droplets of different sizes dispersed within a detonation-product gas mixture at a temperature of 3500K.

The first model utilized was proposed by Butz et al.[26], and assumes that the droplets do not move relative to the gas, that the droplet surface temperature, and the gas far-away temperatures are constant. These conditions correspond to the Nusselt number of 2. The results pertaining to the droplet diameter dependence of the evaporation time, are displayed in Fig.4, the curve labeled "*Butz et al.[26]*".

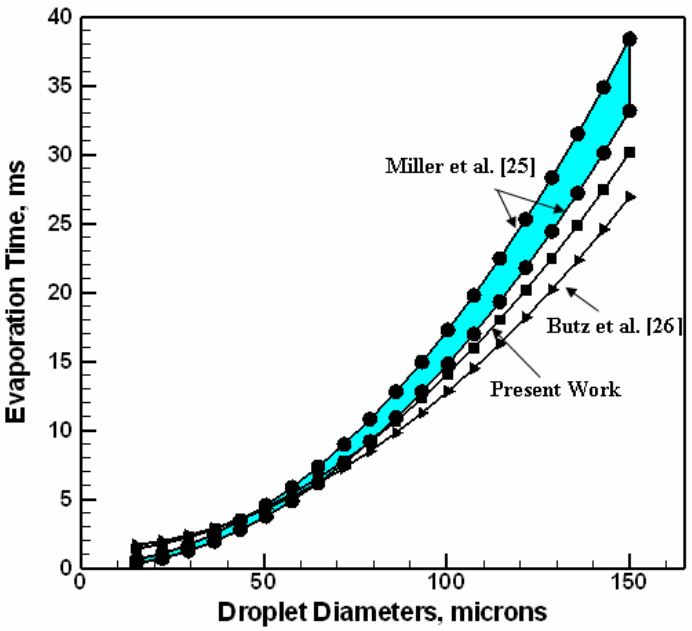

Fig.4. Variation of the simple water-droplet evaporation time with the droplet diameter. Please see text for detail.

The second model was developed in the present work and is briefly described in Appendix A. This model is an extension of the model developed by Butz et al. [26], and includes the effect of droplet heating to the boiling temperature. The results of this analysis are also displayed in Fig.4, the curve labeled, "*Present Work*".

The last model utilized is in fact a series of non-equilibrium evaporation models described by Miller et al. [25]. A brief description of this model is given in Appendix B.

The predictions given by this model are shown in Fig.4, the band labeled *"Miller et al. [25]"*.

The results displayed in Fig.4, suggest that in order for water droplets to be able to evaporate within a time span not greater than 10ms, their diameter should be smaller than ~90μm. The period of 10ms is commonly considered as a time span over which the major portion of the momentum transfer from the detonation-product gas-mixture to the target structure/personal takes place.

3.2 Reduction in the Shock Speed

3.2.1 General Consideration

When water is aerosolized as a result of an interaction with the detonation products of a nearby high-energy explosive, the speed of sound and, thus, the shock speed in the surrounding moisture-laden air becomes substantially reduced [20]. This observation can be rationalized as follows:

(a) The speed of sound in a material can be defined as the square root of a ratio of its bulk modulus, B, and its density, r;

(b) At room temperature, water has a relatively large value of the bulk modulus of $B_{H_2O} = 2.05\times10^9\ Pa$ and a density of approximately $r_{H_2O} = 999 kg/m^3$, and in accordance with the aforementioned relation, the speed of sound is $C_{H_2O} = 1{,}432\ m/s$;

(c) In the frequency range of the sound waves and the shock waves accompanying a detonation event, the bulk modulus of a gas is typically defined as the product of its pressure, P, and the ratio of its constant-pressure and its constant-volume specific heats, g. For a diatomic gas like air, g=1.4, and at the atmospheric pressure P=101.3kPa and at a standard density of $r_{air} = 1.225\ kg/m^3$, the bulk modulus and the speed of sound are: $B_{air} = 1.414\times10^5\ Pa$ and $C_{air} = 340.3 m/s$, respectively;

(d) When water is finely dispersed in air, the speed of sound as a function of the volume fraction of water shows a very interesting behavior as displayed in Fig.5. This behavior arises from the fact that the bulk modulus of the air-water mixture, B_{mix}, is given as:

$$\frac{1}{B_{mix}} = \frac{1-f_{H_2O}}{B_{air}} + \frac{f_{H_2O}}{B_{H_2O}} \tag{16}$$

where f_{H_2O} is the volume fraction of water in the mixture. Eq. (16) reflects the fact that the modulus of the air-water mixture is dominated by the phase present in a larger volume fraction and by the phase that is volumetrically more compliant.

The density of the air-water mixture, r_{mix}, is likewise defined as:

$$r_{mix} = (1-f_{H_2O})\,r_{air} + f_{H_2O}\,r_{H_2O} \tag{17}$$

The variation of the speed of sound in an air-water mixture, C_{mix}, with the volume fraction of water, f_{H_2O}, for the previously stated values of B_{H_2O}, B_{air}, r_{H_2O} and r_{air}, is calculated using the equation $C_{mix}(f_{H_2O}) = \sqrt{B_{mix} / r_{mix}}$.

(e) The results of this calculation are shown in Fig.5. The results displayed in Fig.5 show that the speed of sound in an air-water mixture is substantially reduced and it is below 50m/s for the water volume fraction between 0.06 and 0.94; and

(f) According to the standard normal shock relations, a fixed pressure discontinuity across a shock wave, P_2/P_1, corresponds to a unique value of the Mach number for air or air-water mixture behind the shock wave, M_s. A fixed value of the Mach number at a reduced level of the speed of sound implies a lower speed of air-water mixture moving behind the shock wave as well as a lower speed of the shock wave.

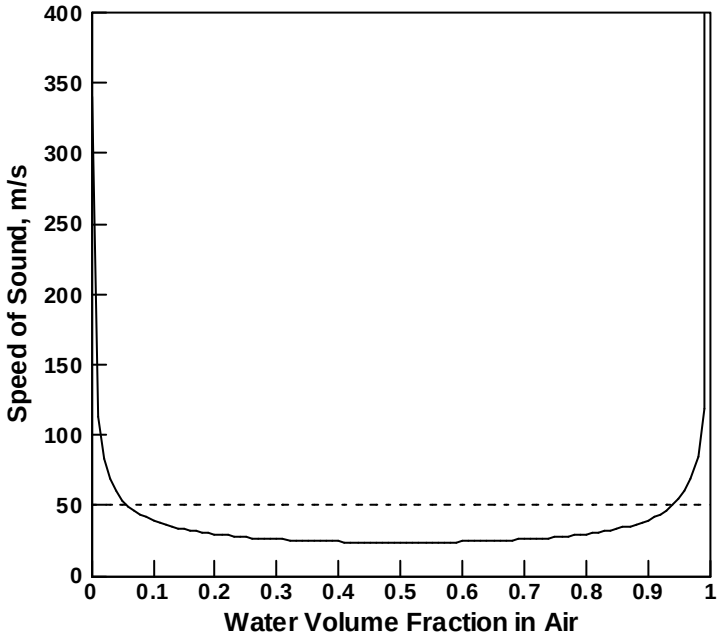

Fig.5. The variation of sound speed in the air/water mixture as a function of the volume fraction of water at the ambient temperature.

3.2.2 A Nonlinear-dynamics Shock-based Analysis

To demonstrate computationally that the presence of moisture in air would indeed reduce the shock speed, a simple Euler-based simulation of a shock-tube experiment is carried out using AUTODYN. Towards that end, a two dimensional Eulerian axisymmetric computational domain with a length-to-diameter ratio of 20:1 is used. One twentieth of the tube length at one of its ends is filled with high-pressure air while the remainder of the tube is filled with either the atmospheric-pressure air or with an air-water mixture containing 50 volume % of water at the atmospheric pressure. Along all

the edges of the computational domain, the "*no-flow*" boundary conditions are applied. Six gage points at equal intervals of 50mm were placed and the pressure at these points recorded during the simulation.

The results pertaining to the pressure-time traces at the six gage points for air and air-water mixture are displayed in Figs 6(a) - (b), respectively. From the shockwave arrival times at the different gage points (the times at which the overpressure reaches the peak value) displayed in Figs 6(a)-(b) and the known locations of the gage points, the average shockwave speeds (and their temporal evolutions) are computed. The ratio of the two average speeds is found to vary between 14.0 and 14.1 as a function of time. A similar ratio is found for the longitudinal velocities of air and the air-water mixture behind the shock wave. These are in excellent agreement with the corresponding ratio of the sound speeds obtained using the procedure described in the previous section $C_{air} / C_{mix} = 340.3 m/s / 23.82 m/s \approx 14.3$.

The results obtained clearly show that the speed at which the air-water mixture moves and ultimately interacts with a structure/personal is reduced. This speed reduction, on one hand, yields longer times over which water break up into droplets and evaporation can take place. On the other hand, as demonstrated in Section 3.3.2, this also causes a reduction in the relative droplet/gas velocity, the parameter which greatly affects the rate of the water break-up process. The presence of these two counteracting effects suggests (in the absence of a detailed numerical analysis) that the shock-speed reduction has, perhaps, a second-order effect on the water break-up and evaporation processes.

The results displayed in Figs 6(a)-(b), show that the presence of water increases the magnitude of the hydrostatic overpressure by around 20%. Even more serious is the potential increase in the dynamic pressure caused by the use of water. The dynamic pressure generally scales with a product of the density of the fluid and the square of its speed. In the present case, the use of 50 volume % of water causes the density to increase by a factor of nearly 500 while the squared velocity would decrease by a factor of $14.3^2 \approx 225$. This finding suggests that the dynamic pressure would in fact increase by a factor (=500/225) greater than 2. It appears, hence, that for the water to display the desired explosion-mitigation effect, it should be dispersed into fine droplets but these droplets should evaporate (before reaching the target) and reduce the temperature and side-on pressure of the detonation-product gas-mixture rather than remain as liquid droplets dispersed within the gas phase.

To demonstrate directly that water-aerosolization induced decrease in the shockwave speed may not have the often-predicted explosion-mitigation effect, a small cylindrical disk shaped target made of 4340 steel is inserted into the shock tube. The axis of the target is set to coincide with that of the tube. The target is modeled as a Lagrangian part and the Euler/Lagrange coupling option inside AUTODYN is used to account for the interaction between the detonation-product gas-mixture (with and without water droplets dispersion) and the target. The temporal evolution of the momentum of the target is monitored in the two cases. It is found that the target momentum is approximately twice as large in the case of the explosion-products gas-mixture containing water droplets, in full agreement with the results of the dynamic-pressure analysis presented above.

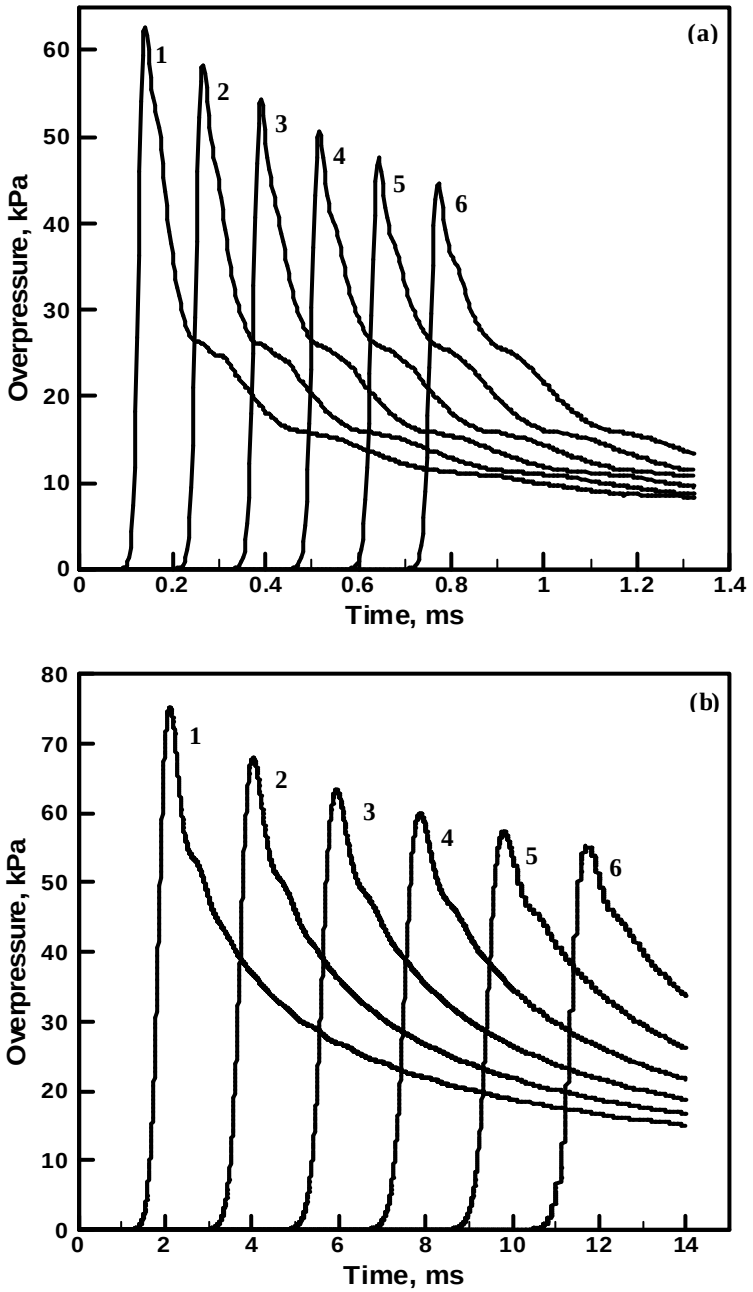

Fig.6. Pressure-time traces at the six gage points 50mm apart located in: **(a)** air and **(b)** air-water mixture inside a shock tube.

3.3 Momentum Transfer

3.3.1 General Consideration

When the detonation front of a high-energy explosive, explosive casing fragments or soil ejecta reach the explosive/water-barrier interface, they creates a positive pressure wave which travels through the water. When this wave reaches the opposite water surface, i.e. the water/air interface, it reflects as a negative-pressure (expansion) wave due to a large acoustic impedance mismatch between water and air. Acoustic impedance is typically defined as a product of the material density and its sound speed and based on the density and sound speed values for air and water reported in Section 3.2.1, the acoustic impedances of water and air are 1.43×10^{6}Rayles and 417.7Rayles, respectively. Thus, there is a significant acoustic impedance mismatch at the water/air interface.

A liquid like water cannot sustain a significant negative pressure and the water region at the water/air interface breaks up into droplets and sprays out into the surrounding air. This process continues as the expansion wave propagates back towards the explosive/water interface. In the process just described, the momentum initially carried by the explosive products, soil ejecta or other debris are transferred to the effectively entire mass of the surrounding water. Consequently, the average velocity at which the water droplets are sprayed out can be a very small fraction of the shock velocity, substantially mitigating the effects of explosion on the surrounding structures/personnel.

3.3.2 Water Fragmentation Computational Analysis

To demonstrate computationally, that the water aerosolization process described above is feasible, a simple SPH (Smooth Particle Hydrodynamics) method based model is developed and solved using AUTODYN. The SPH solver is used because its non-mesh (i.e. particle) based nature gives rise to a more clear visual description of the water aerosolization process.

The rectangular computational domain used in this portion of the work is shown in Fig.7 (a). Within this domain, a semicircular region is filled with TNT while the remainder of the domain is filled with water. The lower edge of the domain is defined as the axis of symmetry, while "*zero-stress*" boundary conditions are applied to the remaining domain edges. A single detonation point is placed at the center of the bottom edge. Two gage points are placed along the vertical midline, as shown in Fig.7 (a) so that a temporal variation of the pressure can be monitored at these points. In addition, field variations of the pressure and the morphology of the computational domain during simulation are also monitored.

Typical results pertaining to the field and temporal variation of the pressure show a circular (compressive) shock wave emanating from the TNT detonation point and propagating toward the opposite long edge of the domain, i.e. the water/air interface. Once the shock wave reaches the opposite long edge of the domain, it reflects as an expansion wave. This behavior is more clearly seen by monitoring the pressure-time traces at the two gage points, as shown in Fig.7 (b). The results shown in Fig.7(b) show that the shock wave arrives first at the gage point 1 which is closer to the TNT charge, while the expansion wave first reaches the gage point 2 which is closer to the water/air interface.

The results pertaining to the morphology of the computational domain are found to be

fairly sensitive to the negative-pressure level selected for the onset of failure in water. In general however, two different aerosolization mechanisms are observed: (a) a "*spalling*" mechanism in which distinct layers of water is spalled-off at the water/air interface, Fig. 8(a) and; (b) a "*water-fragmentation*" process in which water at the water/air interface breaks up into irregular fragments, Fig.8 (b). The former mechanism is typically observed when the least negative values of the failure-pressure are used while the latter is typically observed at the most negative levels of the failure pressure. In the case of water spallation, discrete layers of water are formed and the interlayer gaps, initially containing vacuum, are quickly filled with water vapor. This, in turn, prevents water layers from coming back into a direct contact and further facilitates break-up of the layers into discrete water droplets. In the case of the water-fragmentation process, water fragments freely fly out and undergo further break-up into small-size droplets.

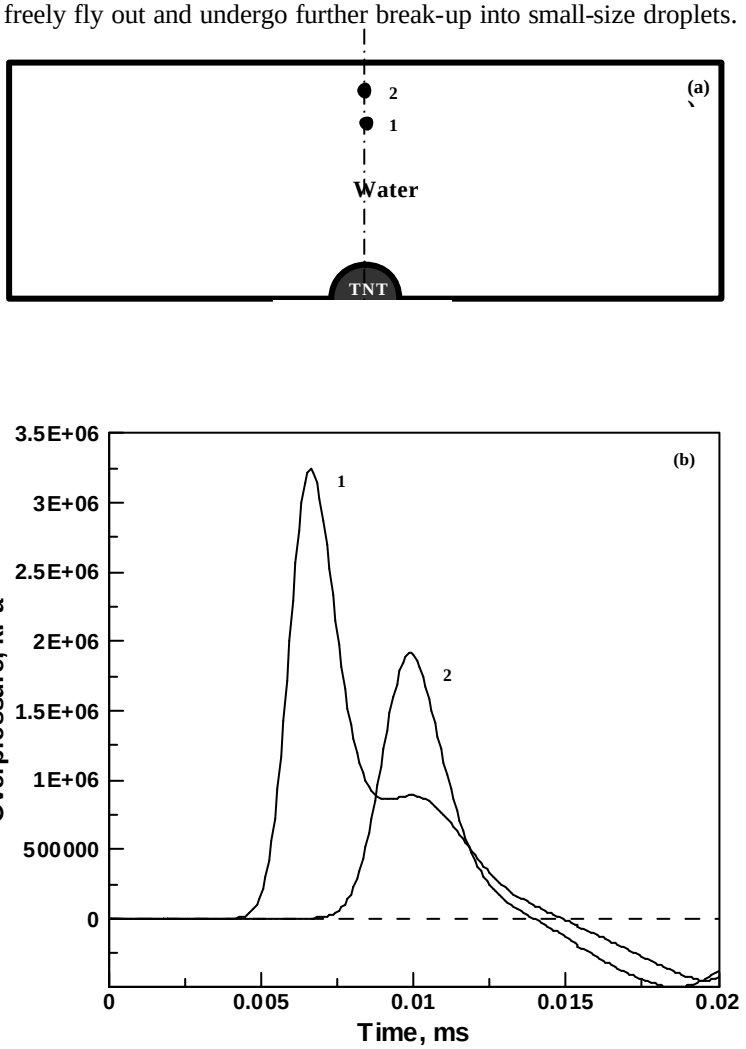

Fig.7. (a) A computational domain used in the SPH (smooth Hydrodynamics) analysis of the water aerosolization process; **(b)** Typical variation of pressure at the two gauge points during simulation.

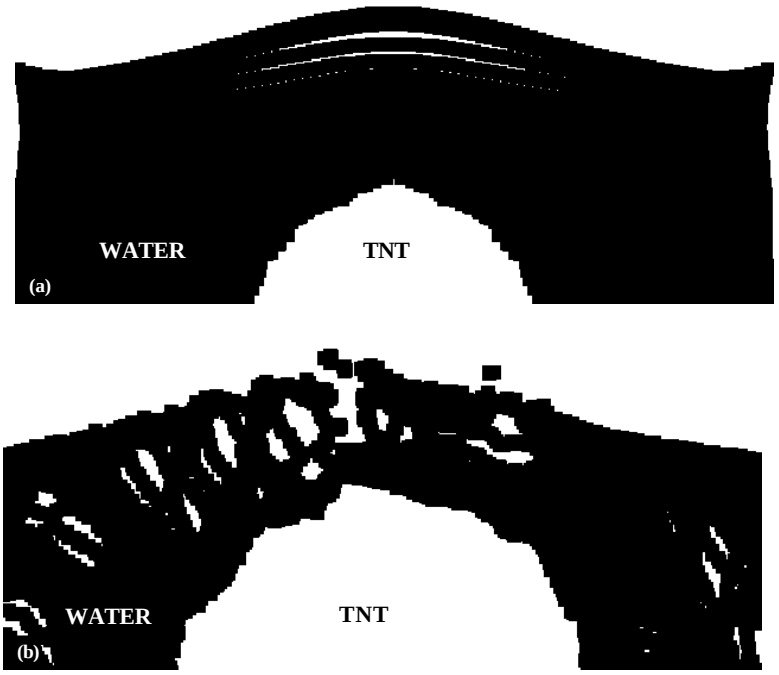

Fig.8. Two mechanisms of water aerosolization: **(a)** a "spallation" mechanism and **(b)** a "fragmentation" mechanism.

The two mechanisms described above can be considered as the mechanism controlling the initial stage of water break-up into larger fragments. Once these fragments are formed, they undergo further break-up into smaller water droplets. A detailed analysis of the subsequent fragment break-up process is not carried out in the present work. Nevertheless, it is well established that there is a number of such fragment break-up mechanisms including bag break-up, multi-mode break-up and shear stripping [21]. A simple schematic of these three fragment break-up mechanisms is displayed in Figs 9(a)-(c). In each case, a spherical droplet (far left) is deformed as a result of its interaction with the aerodynamic forces of the surrounding gas. In the case of the bag break-up mechanism, deformed droplets acquire a thin-wall half-ellipsoid bag shape. During the multi-mode break-up multiple bags are formed and connected to a central column of fluid forming an umbrella-like shape. Within the shear-stripping mode, only the outer layers of the droplets are deformed (sheared off). Which of these mechanisms dominates water breakup into small droplets is controlled by the magnitude of the Weber number, *We*, which is defined as:

$$We = \frac{r_w u^2 d}{s} \tag{18}$$

where r_w is the water density, *?* the velocity of the gas stream relative to that of the

water fragment, d the equivalent droplet diameter and s the water/gas surface energy. It is generally recognized [21-22] that the minimum critical value for the Weber number required for the break-up mechanism to become operative is about 12. Multi-mode break-up and shear stripping mechanisms entail high Weber numbers of approximately 20 and 70, respectively.

Since the water density, ρ_w, and its surface tension can vary only in relatively small ranges, large values of the Weber number are attained according to Eq.(18) at large values of the relative velocity of the gas and at large values of the equivalent droplet diameter. This indicates that the efficiency of the water break-up process is the highest at the shortest post-detonation times and degrades continuously. The attainment of a fine water mist as a result of an interaction between the detonation-product gas-mixture and the bulk water is governed by the magnitude of the explosive's internal energy, since the explosives internal energy controls the initial detonation-product gas velocity. Once a water mist consisting of micron-size droplets is produced, as argued in Section 3.2, the evaporation rate can become significant, causing a major absorption of the energy carried by the detonation-product gas-mixture and a substantial reduction in the gas-phase temperature and pressure. In other words, the momentum transfer from the detonation-product gas-mixture to the bulk water and the subsequent aersolization of the water are the key prerequisites for obtaining the desired explosion-mitigation effect. The actual explosion-mitigation effect, however, appears to be dominated by the water-droplets evaporation process. It is, hence, critical that the water break-up process into micron-size droplets is completed over a short time period (perhaps less than 1ms) to enable a sufficient time for droplet evaporation. Based on the substantial amount of experimental data, the following correlation for the time, t_b, for one break-up event has been proposed [27]:

$$t_b = \frac{d}{u}\sqrt{\frac{\rho_w}{\rho_g}} \cdot \begin{cases} 6(We-12)^{-0.25} & 12 < We < 18 \\ 2.45(We-12)^{-0.25} & 18 < We < 45 \\ 1.41(We-12)^{-0.25} & 45 < We < 351 \end{cases} \tag{19}$$

where ρ_g is the gas density.

As established earlier, the Weber number continuously increases as a function of time following detonation, so that the time for each subsequent break-up event becomes longer and longer. The increase in the Weber number during simulation is being studied by us in an ongoing investigation. Based on the preliminary results of this investigation, and under the assumption that the initial water fragments have an effective diameter of 10mm, the time required to produce water mist with an average droplet diameter of 50μm has been estimated between 0.5 and 2ms. While more work is needed in the ongoing analysis to narrow down this time range, the initial results appear encouraging, with respect to obtaining micron-size water droplets over a time period which is relatively small compared with the droplet evaporation time.

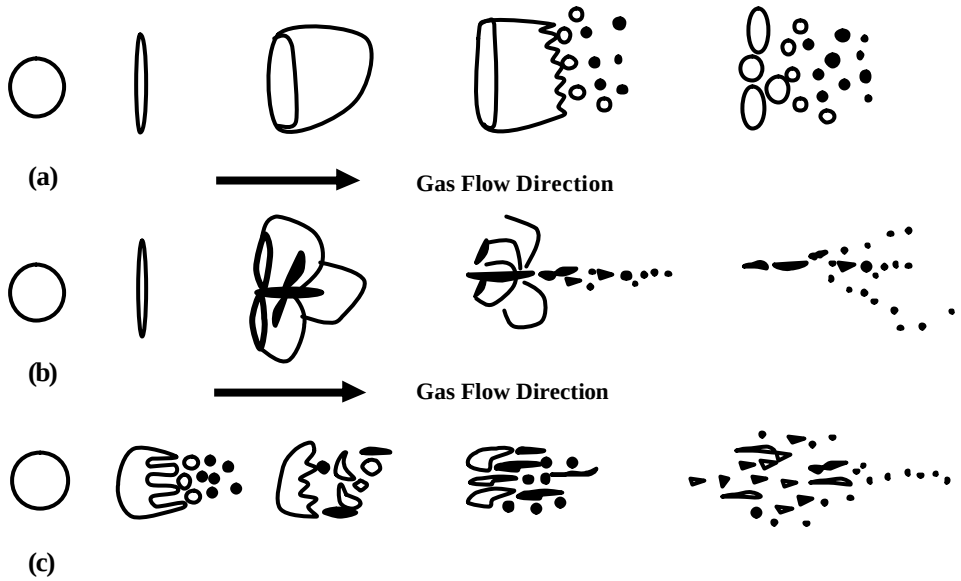

Fig.9.A schematic of three water break-up mechanisms commonly observed: **(a)** Bag break-up; **(b)** Mixed-mode break-up; and **(c)** Shear stripping.

3.4 Deceleration/Suppression of Combustion

3.4.1 General Consideration

Many explosives like TNT are oxygen deficient, i.e. they do not contain enough oxygen to oxidize all the elements in the explosive during an explosion. The detonation reaction of TNT with a chemical formula $C_7H_5N_3O_6$ in the absence of external oxygen can be written as follows:

$$C_7H_5N_3O_6(s) \rightarrow 2.5H_2O(g) + 3.5C(s) + 3.5CO(g) + 1.5N_2(g) + 1.034MJ/moleTNT \quad (20)$$

If at least 5.25 moles of external oxygen are present per one mole of TNT, the detonation products C(s) and CO(g) can be oxidized completely, according to the following reaction:

$$3.5C(s) + 3.5CO(g) + 5.25O_2(g) \rightarrow 7CO_2(g) + 2.373\ MJ/moleTNT \quad (21)$$

where *(s)* and *(g)* are used to denote the solid and the gas phase, respectively.

This reaction typically takes place in two steps: (i) An oxidation of C(s) into CO(g) and (ii) a subsequent oxidation of CO(g) into CO_2(g). A comparison of Eq. (20) and Eq. (21) shows that the total molar heat of combustion of TNT (1.034+2.370 = 3.407MJ/mole TNT) is 3.295 times larger than the molar heat of detonation (1.034MJ/mole TNT). When TNT undergoes only a detonation reaction as defined by Eq.(20), a cloud of finely dispersed soot is typically formed. In sharp contrast, the combustion of carbon and carbon monoxide in accordance with Eq. (21) gives rise to a fireball which expands with the blast front.

It is well established [22] that bulk water or water mist can be very effective in hampering or even preventing the combustion reaction as given by Eq. (21). Typically, no fireball is formed during explosion while air remains clean and water becomes sooty.

While the mechanism by which water hampers/suppresses the combustion reaction is not well understood, two possible explanations are often cited:

(a) As demonstrated earlier, water evaporation can significantly decrease the temperature of the detonation-product gas mixture, and, hence, lower the partial pressure of CO(g) reducing the thermodynamic driving force for the oxidation reaction of CO(g) to CO_2(g); and

(b) The aforementioned reduction in temperature can lower the reaction rate constant and, thus, slow down the kinetics of the combustion reaction as defined by Eq.(21).

A simple quantitative analysis of these two effects is presented in the next section.

3.4.2 A Chemical Thermodynamics and Kinetics Analyses

As explained earlier if one kilogram of water is evaporated for every kilogram of TNT detonated the temperature of the resulting detonation-product gas-mixture would be reduced by about one-third (from ~3500K to ~2300K). A similar reduction in the partial pressure of CO(g) is expected which would reduce the thermodynamic driving force for oxidation of CO(g) into CO_2(g) by one-third. This finding suggests that the water-induced reduction of thermodynamic driving force for the combustion of the detonation products most likely plays a minor role in the overall explosion mitigation effects of water.

In addition to reducing the thermodynamic driving force for combustion, water-induced reduction in temperature of the detonation-product gas-mixture also reduces the rate of the combustion reaction. The forward rate constant for a reaction such as the one shown in Eq. (21) can be defined by the following Arrhenius type relation:

$$k_f = A_2 T^b \exp\left(-\frac{E}{RT}\right) \tag{22}$$

where the pre-exponential term A_2, the temperature exponent b and the activation energy, E, are characteristic parameters for a given chemical reaction, R (= 8.314 J/mol K) is the universal gas constant and T the absolute temperature.

The two elementary reactions associated with the combustion of the detonation-product gas-mixture are:

$$C(s) + 0.5O_2(g) \rightarrow CO(g) \tag{23}$$

$$CO(g) + 0.5O_2(g) \rightarrow CO_2(g) \tag{24}$$

The temperature dependencies of the forward reaction rate constants for the oxidation reactions given by Eqs. (23) and (24) are calculated using the data from Ref.[23] and shown in Fig.10. It should be noted that a logarithmic scale is used along the vertical axis in Fig.10. The results displayed in Fig.10 show that the water-induced reduction in temperature of the detonation-product gas mixture from ~3500K to~2300K gives rise to the corresponding reduction in the forward reaction rate constants of 75% and 96% for the reactions defined by the Eqs.(23) and (24), respectively. These findings indicate that

the water-induced temperature decrease in the detonation-product gas-mixture can substantially reduce the rate of the combustion reaction.

It should be noted that both the oxidation of C(s) given by Eq. (23) and the oxidation of CO(g) given by Eq.(24) are associated with an "*ignition temperature*", i.e., a minimum temperature necessary for the combustion reaction to initiate. The ignition temperatures for C(s) and CO(g) are generally taken as 1173K and 917K, respectively [24]. An extension of the thermo-chemical analysis presented in Section 3.1.2, and the use of the temperature-dependent specific heats displayed in Fig.3 revealed that if 2kgs of water are evaporated for each kilogram of TNT detonated, the temperature of the resulting detonation-product gas-mixture would be around 900K giving rise to a complete suppression of the combustion reaction.

It should also be noted that the chemical-kinetics based analysis presented above is valid under the condition when the combustion reaction is controlled by the rates of the associated oxidation reactions. When the rate of the combustion reaction is controlled by the mass transport of the fuel (C(s) and CO(g)) and oxygen, the presence of water droplets in the combustion-product gas-mixture can affect the extent of turbulence and, in turn, increase the rate of the combustion reaction. This phenomenon was discussed in Section 3.1.2 and is not considered in greater details in this portion of the work. As stated in Section 3.1.2, the effect of water droplets on the extent of turbulence is considered to be of a second order.

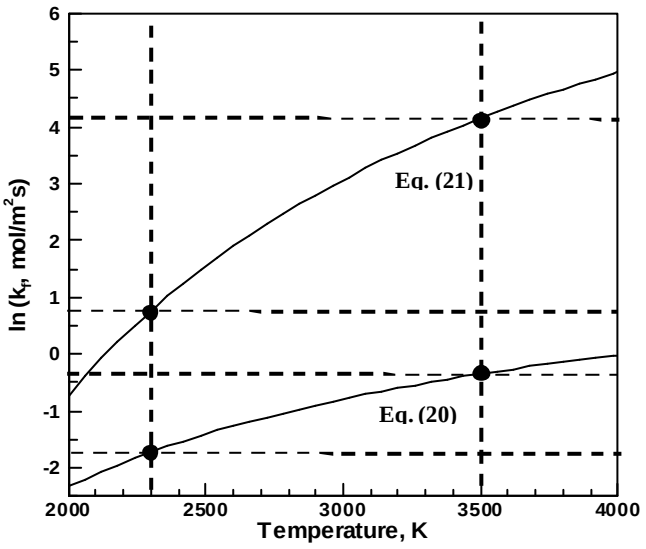

Fig.10. Temperature variation of the logarithm of the rate constants for the forward reactions defined by Eqs. (20) and (21).

4. CONCLUSIONS

Based on the results obtained in the present work, the following main conclusions can be drawn:

1. Among the four water-induced explosive-mitigation mechanisms studied in the present work, water evaporation which absorbs the major portion of the thermal energy carried by the detonation-product appears to be the dominant mechanism. Water evaporation reduces the temperature and pressure of the detonation-product gases and can prevent their combustion.
2. The presence of water vapor in the gas phase has also an explosion-mitigation effect through the potential reduction of the thermodynamic driving force for the combustion reaction.
3. The transfer of momentum from the detonation-product gas-mixture to water is a key phenomenon controlling the break-up of water into micron-size droplets. Consequently, this process acts as a prerequisite for an effective explosion-mitigation via water evaporation.
4. While the role of the reduced shock speed caused by the presence of water droplets in the detonation-product gas-mixture in explosion mitigation was not analyzed quantitatively, it appears to be of a second order.

ACKNOWLEDGEMENTS

The material presented in this paper is based on work supported by the U.S. Army/Clemson University Cooperative Agreement W911NF-04-2-0024 and by the U.S. Army Grant Number DAAD19-01-1-0661. The authors are indebted to Drs. Walter Roy and Fred Stanton for the support and a continuing interest in the present work.

Appendix A: Rate of Evaporation of Water Droplets

In this section, a simple model is developed for an assessment of the rate at which water droplets evaporate when dispersed within hot detonation-product gas-mixture. The model developed is based on the following simplifications and assumptions:

(a) Water droplets are spherical in shape and all have the same radius, R;
(b) Water droplets are distributed uniformly within the detonation-product gas-mixture so that it can be assumed that each single water droplet resides within a cube with an edge length, l. The cubes are distributed uniformly in space. Then each cube is replaced with a sphere of an equal volume with a radius, $a = (3/4\pi)^{1/3} l$. Since each such spherical cell is identical, there is no heat flux across its surfaces.
(c) The volume fraction of the water in the gas mixture can be then defined as $f_{H_2O} = (R/a)^3$; and
(d) Due to the intrinsic spherical symmetry of the problem as posed above, a one-dimensional mathematical model within the spherical coordinate system can be used.

The problem defined above can be mathematically expressed by the following energy conservation equation:

$$\rho_{gas} C_{P,\,gas} \frac{\partial T}{\partial t} = k_{gas} \left(\frac{1}{r} \frac{\partial T}{\partial r} + \frac{\partial^2 T}{\partial r^2} \right) \tag{A.1}$$

subject to the initial conditions:

$$T(r > R,\ t = 0) = T_{init,\,gas} \tag{A.2}$$

$$T(r \le R,\ t = 0) = T_{init,\,H_2O} \tag{A.3}$$

and the boundary conditions:

$$k_{gas}\left.\frac{\partial T}{\partial r}\right|_{r=a} = 0 \tag{A.4}$$

$$k_{gas}\left.\frac{\partial T}{\partial r}\right|_{r=R} \cdot A_{H_2O} = r_{H_2O} C_{P,H_2O} \dot{T}_{H_2O} V_{H_2O} \quad \text{for } T_{H_2O} < T_{H_2O,boil}, \text{ and} \tag{A.5}$$

$$k_{gas}\left.\frac{\partial T}{\partial r}\right|_{r=R} \cdot A_{H_2O} = r_{H_2O} L_{H_2O} \dot{V}_{H_2O} \text{ for } T_{H_2O} = T_{H_2O,boil}, \tag{A.6}$$

where, r is density, C_P constant-pressure specific heat, k thermal conductivity, T temperature, r spatial coordinate, L latent heat of evaporation, A surface area, V volume, subscripts "*gas*" and "*H2O*" are used to denote the quantities pertaining to gas and water droplets, respectively, while a raised dot is used to denote the first time derivative of a quantity.

The boundary condition defined by Eq. (A.5) is used while water droplets are heated up to their boiling point, $T_{H_2O,boil}$, while Eq. (A.6) is used for the case when water droplets are at $T_{H_2O,boil}$ and evaporation occurs.

Eqs. (A.1) – (A.6) are solved using an explicit finite-difference procedure. A standard mesh convergence analysis is carried out to ensure that the effect of the mesh size has been essentially eliminated. The results of this analysis, however, will not be presented here for brevity.

Appendix B: Non-equilibrium Liquid Droplet Evaporation Model

In a recent paper, Miller et al. [25] carried out a comprehensive overview of the existing non-equilibrium two-phase models for evaporation of a liquid phase dispersed in the form of single-species spherical droplets. The droplets exchange their momentum with the surrounding carrier gas only via the drag forces, while the thermal energy is exchanged only via the convective heat transfer. The models had to be modified before they can be used in the present case in order to include the assumption that the droplets are stationary relative to surrounding gas. Under these conditions, evaporation of a simple droplet is defined by the droplet temperature, T_d, and the droplet mass, m_d, evolution equations as:

$$\frac{dT_d}{dt} = \frac{f_2 Nu}{3\,\mathrm{Pr}_G}\left(\frac{q_1}{t_d}\right)(T_G - T_d) + \left(\frac{L}{C_L}\right)\frac{\dot{m}_d}{m_d} - H_{\Delta T} \tag{B.1}$$

and

$$\frac{dm_d}{dt} = -\frac{Sh}{3Sc_G}\left(\frac{m_d}{t_d}\right)H_M \qquad \text{(B.2)}$$

where $\dot{m}_d = \frac{dm_d}{dt}$ (negative for evaporation), T_G is the local carrier-gas temperature, L the latent heat of evaporation, $q_1 = C_{p,G} / C_L$ is the ratio of the constant-pressure gas heat capacity, $C_{p,G}$, to that of the liquid phase C_L, the gas-phase Prandtl, $\mathrm{Pr}_G = mC_{p,G} / l_G$, and Schmidt, $Sc_G = m_G / r_G D_G$, numbers, m gas-phase viscosity, l gas-phase thermal conductivity, D binary gas-phase diffusion coefficient and r_G gas-phase density. The subscripts denote the droplet (*d*), gas-phase property away from the droplet surface (*G*), vapor phase (*V*), and liquid phase (*L*). In Eqs. (B.1) and (B.2), $t_d = r_d d^2/(18m_G)$ is the particle time constant for Stokes flow, where d is the droplet diameter, and f_2 is a heat transfer correction due to evaporation, and the Nusselt (*Nu*) and Sherwood (*Sh*) numbers are empirically modified for convective corrections to heat and mass transfer, respectively. Finally, $H_{?T}$ accounts for all additional terms used to incorporate non-uniform internal temperature effects (i.e. finite liquid thermal conductivity), and H_M represents the specific driving potential for mass transfer (analogous to T_G-T_d for heat transfer).

Eqs. (B.1) and (B.2) have been cast into these specific forms in order to highlight the fact that various models proposed in the literature differ predominantly with respect to how the parameters f_2, H_M and $H_{?T}$ are calculated. Five different models (denoted as M3-M7 in Ref. [25]) were implemented into present work and using the same numerical procedure described in Appendix A.

REFERENCES

[1]. P. A. Tatem, C. L. Beyler, P. J. DiNenno, E. K. Budnick, G. G. Back, and S. E. Younis, *A Review of Water Mist Technology for Fire Suppression*, NRL/MR/6180-94-7624, Naval Research Laboratory, 1994.

[2]. G. G. Back, P. J. DiNenno, J. T. Leonard, and R. L. Darwin, *Full Scale Tests of Water Mist Fire Suppression Systems for Navy Shipboard Machinery Spaces: Phase I - Unobstructed Spaces*, NRL/MR/ 6180-96-7830, Naval Research Laboratory, March 1996.

[3]. G. G. Back, P. J. DiNenno, J. T. Leonard, and R. L. Darwin, *Full Scale Tests of Water Mist Fire Suppression Systems for Navy Shipboard Machinery Spaces: Phase II - Obstructed Spaces*, NRL/MR/ 6180-96-7830, Naval Research Laboratory, March 1996.

[4]. F. W. Williams, G. G. Back, P. J. DiNenno, R. L. Darwin, S. A. Hill, B. J. Havlovick, T. A. Toomey, J. P. Farley, and J. M. Hill, *Full-Scale Machinery Space Water Mist Test: Final Design Validation*, NRL/MR/6180--99-8380, Naval Research Laboratory, June 1999.

[5]. Guidelines for Evaluating the Characteristics of Vapor Cloud Explosions, Flash Fires, and BLEVEs, *Center for Chemical Process Safety*, AIChE, New York, NY, 1994.

[6]. Liebman and J. K. Richmond, Suppression of Coal Dust Explosions by Passive Water Barriers in a single Entry Mine, *U.S. Bureau of Mines* R.I. 8294, 1974.

[7]. Liebman, J. Corry and J. K. Richmond, Water Barriers for Suppressing Coal Dust Explosions, *U.S. Bureau of Mines* R.I. 8170, 1976.

[8]. D-B Zhou and J-Z Lu, Research on the Suppression of Coal Dust Explosions by Water Barriers, in Industrial Dust Explosions, (Ed: K. L. Cashdollar and M. Herzberg), *American Society For Testing and Materials*, PA., 1987.

[9]. D. Ng, M. Sapko, A. Furno and R. Pro, Coal Dust and Gas Explosion Suppression by Barriers", in Industrial Dust Explosions, (Ed: K. L. Cashdollar and M. Herzberg), *American Society For Testing and Materials*, PA., (1987)152-157.

[10]. P. Roman, F. Bana, E. Hindorean and S. Tat, Experiments Concerning the General Use of Water Barriers with Breakable Troughs in Romainia's Gassy Mines, Paper E4, *presented at the 20th International Conference on Safty in Mines*, Sheffield, U.K., Oct. 3-7, 1983.

[11]. W. A. Keenan and P. C.Wager, Mitigation of Confined Explosion Effects by Placing Water in Proximity of Explosives, *25th DoD Explosives Safety Seminar*, Anaheim, CA, 18-20 August 1992.

[12]. S. Eriksson and B. Vretblad, Blast Mitigation in Confined Spaces by Energy Absorbing Materials, *26th DDESB Seminar*, Miami, FL, 16-18 August 1994.

[13]. S. H. Salter, Why is Water so Good at Suppressing the Effects of Explosion?, *UK Explosives Mitigation Workshop*, RCMS Shrivenham, 19 June 2002.

[14]. MATLAB, 6th Edition, The Language of Technical Computing, *The MathWorks Inc.*, 24 Prime Park Way, Natick, MA, 01760-1500, 2003.

[15]. *AUTODYN-2D and 3D*, Version 5.0, User Documentation, Century Dynamics Inc., 2004.

[16]. B. K. Hodge and Keith Koenig, *Compressible Fluid Dynamics*, Prentice Hall, Englewood Cliffs, New Jersey, 1995.

[17]. E. L. Lee, H. C. Hornig and J. W. Kury, Adiabatic Expansion of High Explosive Detonation Products, UCRL – 50422, *Lawrence Radiation Laboratory*, University of California, 1968.

[18]. P. W. Cooper, *Explosives Engineering*, Wiley-VCH, New York, 1996.

[19]. K. Morgan, An Expansion Equation of State Subroutine, *Comp. Phys. Comm.*, pp. 64-68, 5, North-Holland, 1973.

[20]. P. K. Bowyer, F. Hearn, D. Morgan, A. Stockdale and F. Wight, Mitigation of Blast and Fragmentation for Projectiles up to 155mm Using Water Based Tamping, *Final report to RMCS Shrivenham ATO course number 40. 2000*.

[21]. W. R. Lane, Shatter of Drops in Streams of Air, *Ind. Eng. Chem.*, 43(1951)1312.

[22]. K. Kailasanath, *Blast Mitigation Using Water – A Status Report*, NRL/MR/6410--02-8606, Naval Research Laboratory, March 2002.

[23]. *CHEMKIN III*, User Manual, Sandia National Laboratories, San Diego, CA 1996.

[24]. V. Babrauskas, *Ignition Handbook*, Fire Science Publishers, Issaquah WA, 2003.

[25]. R. S. Miller, K. Harstad and J. Bellan, Evaluation of equilibrium and non-equilibrium evaporation models for many-droplet gas-liquid flow simulations, *International Journal of Multiphase Flow*, 24 (1998)1025-1055.

[26]. J. R. Butz and P. French, Application of Fine Water Mists to Hydrogen Deflagration, *Proceedings-Halon Alternatives Technical Working Conference*, Albuquerque, N.M., May 1993.

[27]. R. Schmehl, G. Maier and S. Wittig, CFD Analysis of Fuel Atomization, Secondary Droplet Breakup and Spray Dispersion in Premix Duct of a LPP Combustor, *Eighth Annual Conference on Liquid Atomization and Spray Systems*, Pasadena, CA, 2000.